



OPEN

# Duffing oscillation-induced reversal of magnetic vortex core by a resonant perpendicular magnetic field

SUBJECT AREAS:  
MAGNETIC PROPERTIES  
AND MATERIALS  
MAGNETIC DEVICES  
SPINTRONICS

Kyoung-Woong Moon<sup>1</sup>, Byong Sun Chun<sup>1</sup>, Wondong Kim<sup>1</sup>, Z. Q. Qiu<sup>2</sup> & Chanyong Hwang<sup>1</sup>

Received  
11 June 2014

Accepted  
4 August 2014

Published  
22 August 2014

Correspondence and  
requests for materials  
should be addressed to  
C.H. (cyhwang@kriss.  
re.kr)

<sup>1</sup>Center for Nanometrology, Korea Research Institute of Standards and Science, Daejeon 305-340, Republic of Korea, <sup>2</sup>Physics Department, University of California at Berkeley, Berkeley, California 94720, U.S.A.

**Nonlinear dynamics of the magnetic vortex state in a circular nanodisk was studied under a perpendicular alternating magnetic field that excites the radial modes of the magnetic resonance. Here, we show that as the oscillating frequency is swept down from a frequency higher than the eigenfrequency, the amplitude of the radial mode is almost doubled to the amplitude at the fixed resonance frequency. This amplitude has a hysteresis vs. frequency sweeping direction. Our result showed that this phenomenon was due to a Duffing-type nonlinear resonance. Consequently, the amplitude enhancement reduced the vortex core-switching magnetic field to well below 10 mT. A theoretical model corresponding to the Duffing oscillator was developed from the Landau–Lifshitz–Gilbert equation to explore the physical origin of the simulation result. This work provides a new pathway for the switching of the magnetic vortex core polarity in future magnetic storage devices.**

A magnetic vortex state<sup>1,2</sup> is a ground state of a magnetic nanostructure that consists of a perpendicularly magnetized core and in-plane curling magnetizations around the core (Fig. 1a). Because of its importance in fundamental physics, research on the vortex state is an important emerging topic in magnetism studies<sup>1–7</sup> and it has a high potential for application in high-density data storage devices<sup>5–13</sup>. A magnetic vortex state is energetically fourfold degenerated, which is determined by its polarity and chirality, where the polarity refers to the perpendicular direction of the core magnetization,  $p_{\text{core}}$  (with a value of +1 for the upward direction, or –1 for the downward direction) and the chirality,  $c$ , refers to the curling direction of the in-plane magnetization (a value of +1 or –1 for the counterclockwise or clockwise directions, respectively). Obviously, the success of a magnetic vortex device will critically depend on the question of how to control the vortex polarity and chirality effectively. Much effort has been invested recently in developing various methods for reversing the vortex polarity and chirality with a low magnetic field. While the chirality can be reversed easily with a weak field of ~50 mT (ref. 13), the magnetic field required to reverse the vortex core is on the order of 500 mT, which is too large for practical use in device applications<sup>14–17</sup>.

To reduce the vortex core-reversal field, an alternative approach used a dynamic field<sup>16–10,13,16–23</sup>. The chirality reversal field can be almost halved when a short-pulsed field is applied<sup>13</sup>. A promising result is also reported for an AC oscillating magnetic field set at the vortex resonance frequency, so that the vortex excitation could assist its polarity reversal. A representative example of such an approach is the vortex gyration excitation, in which the vortex core exhibits a spiral motion as an AC magnetic field is tuned on at the gyration eigenfrequency<sup>6–10,19,21</sup>. Core switching occurs subsequently through vortex–antivortex creation and annihilation<sup>6</sup> as the core’s moving speed exceeds a critical value<sup>19</sup>. The core reversal field can be reduced in such a manner to values far below 10 mT (refs 6,7,19).

However, this method contains a fundamental problem for applications. After the core reversal and turning off the field, the core gyration exponentially decays to its initial position. The decay radius is comparable to the lateral size of the sample and the relaxation takes a few hundred nanoseconds<sup>21</sup>. This is a severe obstacle to reading the polarity<sup>16</sup>.

Recently, Wang and Dong<sup>16</sup> and Yoo *et al.*<sup>17</sup> found a new method of vortex core flip from numerical simulation. They demonstrated that the vortex core polarity could be switched in a radial excitation mode<sup>16,17,24,25</sup> by a perpendicular AC magnetic field. In contrast to the gyration mode-assisted switching, which involves the vortex core motion, the radial mode-assisted core switching involves only axial symmetric oscillations, thus preserving the vortex core position. Obviously, the radial mode-assisted core switching has a completely different mech-

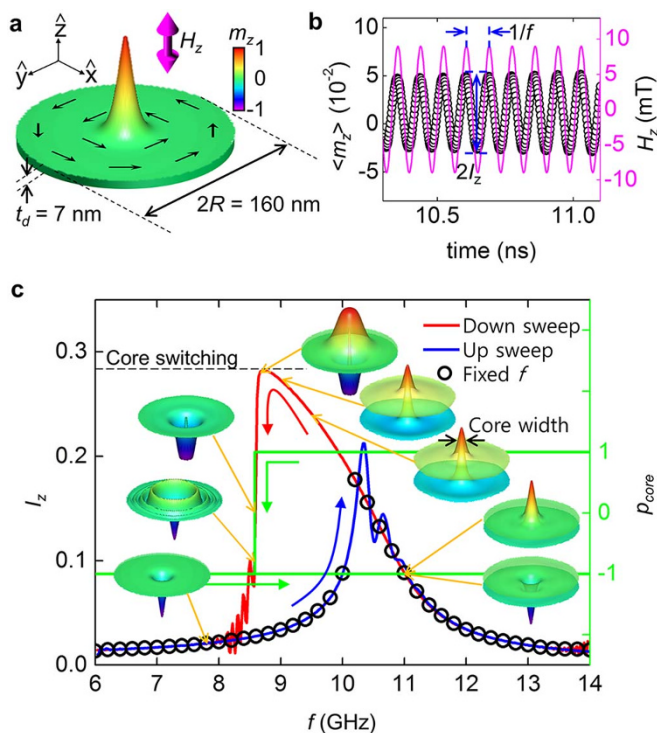


**Figure 1 | Magnetic vortex and core reversal induced by sweeping frequency.** (a), Disk structure used for simulations and the initial vortex state. The in-plane curling magnetization directions are shown as arrows. At the disk center, a perpendicularly magnetized core exists. (b), The magnetization oscillation induced by the external magnetic field  $H_z$  applied to the thickness direction ( $\hat{z}$ ). The field strength was 9 mT with a sinusoidal form; the frequency was varied with 0.2 GHz/ns rate;  $\langle m_z \rangle$  is the spatially averaged magnetization component in the  $\hat{z}$  direction normalized by the saturation magnetization. (c),  $I_z$ , the amplitude of  $\langle m_z \rangle$  oscillation, as a function of external field frequency  $f$ . The amplitude obtained from downward sweeping (red line) can achieve sufficient amplitude for core polarity ( $p_{\text{core}}$ ) reversal but from upward sweeping (blue line) it cannot. Black circles denote saturated amplitude per each frequency. This fixed frequency result also does not obtain the maximum amplitude for  $p_{\text{core}}$  switching. Snap shots show the magnetization states. The overlapped images represent one cycle of the oscillation and single images exhibit the reversal process of the core.

anism from the gyration mode-assisted core switching. The underlying mechanism of the radial mode-assisted core switching was not clearly shown by the simulation. The critical field obtained by the radial mode in these studies is of the order of 20 mT (ref 17), larger than the gyration mode-assisted core reversal.

In this work, we studied the underlying mechanism of the radial mode oscillation and outlined a new pathway to reduce the core-switching field further down to the mT range, which was more comparable to the critical field of the gyration-assisted core switching. In addition to micromagnetic simulations<sup>26</sup>, we also established a dynamical equation for the radial mode oscillation from the Landau–Lifshitz–Gilbert (LLG) equation<sup>27</sup>. This equation clearly explores the nonlinear behavior of the radial mode and the critical field reduction.

For direct comparison of the critical field reduction, the simulation structure was set as described by Yoo *et al.*<sup>17</sup> (Fig. 1a). According to previous studies, the radial modes are classified by the node number  $n$  (refs 17,24). The first mode has one node, the vortex core, which means that the magnetization does not oscillate temporally at the vortex core, but the other parts almost uniformly oscillate. The second mode has two nodes; one is the vortex core and

the other a concentric circle. Yoo *et al.*<sup>17</sup> studied the resonance frequency of the individual radial mode and obtained the eigenfrequencies with the same sample structure as in this study: 10.7 GHz for the first mode ( $n = 1$ ), 15.2 GHz for the second mode ( $n = 2$ ), and 20.7 GHz for the third mode ( $n = 3$ ). They also showed the vortex core polarity reversal using the first mode with an oscillating external field of 20 mT.

To reduce the radial mode-induced critical field below 10 mT, we stimulated the first mode of the radial oscillation with a different method; that is, sweeping of the external field frequency. The field was sinusoidal with amplitude of 9 mT and the field frequency  $f$  was slowly varied from 14.0 to 6.0 GHz over 40 ns. Figure 1b shows the magnetization oscillation during frequency sweeping with time. The normalized magnetization along the thickness direction  $m_z$  and the external magnetic field,  $H_z$ , were plotted together. The term  $\langle m_z \rangle$  means the spatial average over the entire disk. The magnetization oscillation has the same frequency despite the phase difference. From this oscillation, we can get the oscillation amplitude of magnetization,  $I_z$ , in the thickness direction, which is half the difference between the nearest maximum and minimum values of the  $\langle m_z \rangle$  oscillation. After reaching an external field frequency of 6.0 GHz, the frequency sweeping direction was reversed and  $f$  returned to 14.0 GHz.

In Fig. 1c,  $I_z$  is shown as a function of  $f$ . It is interesting to note that an external field of 9 mT can reverse the vortex core polarity. In downward sweeping of the frequency, the almost uniform magnetization oscillation was observed on the disk except for the core conserving its width (inset of Fig. 1c). This uniform oscillation was maintained before  $I_z$  reached the maximum amplitude of 0.28 when  $f$  was 8.7 GHz. After reaching this critical amplitude, the uniform oscillation collapsed and converged into the disk center that generated a breathing motion of the core. Such a breathing generated a strong exchange field when the core was compressed, and then core polarization switching occurred<sup>16,17</sup>. Amplitude fluctuations near 8.5 GHz and 10.5 GHz are transition effects discussed below. In contrast to downward sweeping, the upward frequency sweeping did not reach the amplitude of 0.28, so the vortex maintained its polarity. This means that one cycle of frequency sweeping generated one core reversal. It is notable that the amplitude obtained with the fixed-field frequencies was the same as the upward sweeping. The fixed-field frequency amplitudes were determined by amplitude saturation after turning on the external oscillating field. To reverse the core polarity with the upward sweeping oscillation and fixed-frequency oscillation, a larger field was required for achieving the sufficient oscillation amplitude. From this sweeping frequency simulation, it was verified that the critical field was reduced to below 10 mT and this reduction was only observed in downward sweeping because of the hysteresis behavior of the frequency.

To study this hysteresis behavior, we constructed a simplified model. The magnetization oscillation of the first mode can be represented by only two variables,  $\theta$  and  $\varphi$ , because with the exception of the core region, the magnetization oscillates almost uniformly<sup>17</sup>. Figure 2a shows the definition of  $\theta$  and  $\varphi$  in the core-free model. The angle  $\theta$  represents the magnetization tilting toward the normal direction and  $\varphi$  denotes tilting in the radial direction. The initial magnetization is then described as  $\theta = 0$  and  $\varphi = 0$ . Note that the initial magnetization of the vortex state could have two values of  $\varphi$ , 0 and  $\pi$ , because of the chirality of the vortex. The two states are energetically equivalent, so in this paper we only considered  $\varphi = 0$  as the initial state. Using these two variables, the magnetization state of each component was described as  $M_r = M_S \cos\theta \sin\varphi$ ,  $M_\varphi = M_S \cos\theta \cos\varphi$ , and  $M_z = M_S \sin\theta$ . After inserting these components into the LLG equation<sup>27</sup> and solving, we could derive the following coupled equations:

$$\dot{\varphi} = \gamma M_S (N_z - N_r \sin^2 \varphi) \sin \theta + \gamma H \sin \omega t + \frac{\alpha}{\cos \theta} \dot{\theta}, \quad (1)$$

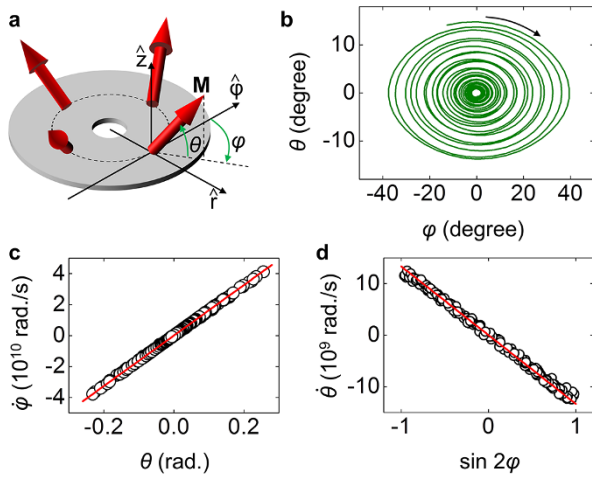


**Figure 2 | Simplified model for the first radial mode.** (a), The angle  $\theta$  is tilting toward the perpendicular direction and  $\varphi$  represents the radial directional tilt. (b), A spiral trajectory during relaxation; before the relaxation, several Gaussian pulses were applied to excite the magnetization oscillation. (c),(d), Relations between two coupled variables,  $\theta$  and  $\varphi$ , which were obtained from (b).

$$\dot{\theta} = -\gamma M_S N_r \cos \theta \sin \varphi \cos \varphi - \alpha \cos \theta \dot{\varphi}. \quad (2)$$

Here, the over dot means the time derivative,  $\gamma$  is the gyromagnetic ratio,  $N_z$  and  $N_r$  are determined by the demagnetizing energy along the  $\hat{z}$  and  $\hat{r}$  directions, respectively,  $H$  is the external field amplitude, and  $\omega (= 2\pi f)$  is the angular frequency of the external field. In equations (1) and (2), all the parameters are known except for  $N_z$  and  $N_r$ . To obtain these two parameters, we reduced equations (1) and (2) assuming that  $N_z \gg N_r$  because of the thin structure, and this condition also results in  $\theta \ll 1$ , after which simplified equations are derived:

$$\dot{\varphi} = \gamma M_S N_z \theta + \gamma H \sin \omega t + \alpha \dot{\theta}, \quad (3)$$

$$\dot{\theta} = -\frac{1}{2} \gamma M_S N_r \sin 2\varphi - \alpha \dot{\varphi}. \quad (4)$$

We carried out a simulation that solved equations (3) and (4). Gaussian-shaped external field pulses were applied sequentially to the nanodisk to excite the first mode and the interval between pulses was tuned for precise resonant amplification<sup>21</sup>. We turned off the external field pulse and observed the relaxation process (Fig. 2b). The angles  $\theta$  and  $\varphi$  converged exponentially to zero with a spiral trajectory;  $\theta$  was obtained from  $\sin \theta = \langle m_z(t) \rangle - \langle m_z(0) \rangle$ , where,  $t$  is time and  $\varphi$  was determined by the averaged value over the entire disk. From this spiral relaxation,  $\dot{\varphi}$  was plotted as a function of  $\theta$  (Fig. 2c) and  $\sin 2\varphi$  was plotted with  $\dot{\theta}$  (Fig. 2d). The damping effect was negligible because  $\alpha = 0.01$  ( $\ll 1$ ) and during relaxation,  $H = 0$ . Thus, two linear relations (Fig. 2c and 2d) determined the values  $N_z = 0.85$  and  $N_r = 0.14$ . These values are reasonable because  $N_z + N_r \approx 1$  for the first mode was composed with almost uniform magnetization.

Next, we solved equations (3) and (4) to obtain the oscillation amplitudes versus the external field frequencies. The time derivative of the equations and the elimination of the  $\dot{\theta}$  and  $\ddot{\theta}$  terms yielded the following equation of motion of  $\varphi$ :

$$(1 + \alpha^2) \ddot{\varphi} + \frac{\omega_0^2}{2} \sin 2\varphi + C(N_z + N_r) \dot{\varphi} - C(2N_r \sin^2 \varphi) \dot{\varphi} - \gamma H \omega \cos \omega t = 0. \quad (5)$$

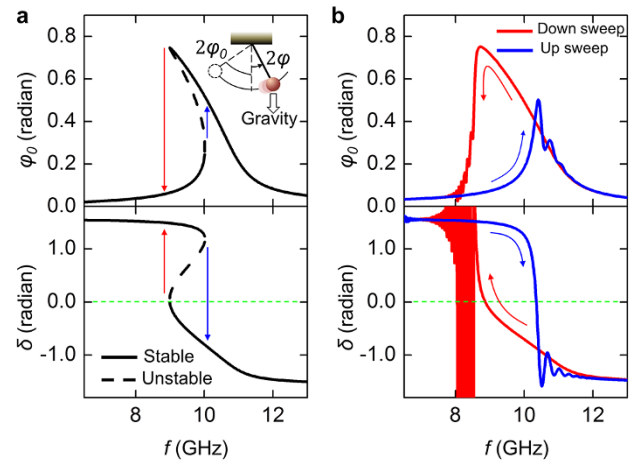


**Figure 3 | Comparison between solutions of the Duffing equation and simulations.** The external field was set to be 8 mT. (a), Solutions of equation (6), the Duffing equation. The plane pendulum asymptotically corresponds to the Duffing oscillator (inset). The solution comprises a stable and an unstable line and where the stable line is disconnected, the amplitude  $\varphi_0$  and the phase  $\delta$  show drastic jumps.  $\varphi_0$  has the maximum value  $\varphi_{\max}$  at the zero phase ( $\delta = 0$ ). (b), Micromagnetic simulation results with the same external field show similar hysteresis behavior.

Here,  $\omega_0 = \gamma M_S \sqrt{N_z N_r} = 2\pi \times 10.7$  GHz and  $C = \alpha \gamma M_S$ . If we neglect the damping term and the external field term, equation (5) exactly corresponds to the simple plane pendulum,  $\ddot{\Phi} + \omega_0^2 \sin \Phi = 0$  with  $\Phi = 2\varphi$ , so it was natural for the main dynamics of the radial mode of the vortex to be the same as that of the plane pendulum. Directly solving equation (5) was not easy, so we simplified equation (5). Firstly, we compared the third and the fourth terms of equation (5), both terms have  $\dot{\varphi}$  dependence, and we neglected the fourth term which is much smaller than the third term. Then, we expanded  $\sin 2\varphi$  in the second term by using a Taylor expansion such as  $\sin x = x - x^3/3! + x^5/5! \dots$  and we adopted up to the third order of this expansion. These simplifications produced the following equation.

$$\ddot{\varphi} + \omega_0^2 \varphi (1 + \beta \varphi^2) + d\dot{\varphi} - F \omega \cos \omega t = 0. \quad (6)$$

This is the well-known Duffing oscillator equation<sup>28,29</sup> that describes a nonlinear oscillation induced by the  $\varphi$  variation-dependent spring constant. If  $\beta = 0$ , equation (6) becomes a harmonic oscillator. In this study,  $\beta = -2/3$  due to the Taylor expansion of  $\sin 2\varphi$ . Other parameters were determined similarly: the dissipative constant  $d = \alpha \gamma M_S (N_z + N_r)$  and the external force  $F = \gamma H$ . It is well known that we can solve the Duffing equation by using the van der Pol transformation<sup>29,30</sup>.

A solution of equation (6), the frequency-dependent amplitude  $\varphi_0$ , exhibits hysteresis behavior (Fig. 3a). We set  $H$  to be 8 mT. In contrast to a harmonic oscillator showing a symmetric resonant peak, the Duffing oscillator exhibits an asymmetric resonance peak and the curve is divided into stable and unstable solutions that are well known as the foldover effect. If we apply the external field with a starting frequency of 14 GHz and monotonically reduce the frequency, the oscillation amplitude would follow the stable solution line until it meets the maximum amplitude point  $\varphi_{\max}$ . After passing the maximum point, the amplitude was drastically reduced to follow the stable line. A similar behavior was also expected for the case of increasing frequency, but the amplitude did not reach  $\varphi_{\max}$  because the stable line was connected up to 10 GHz. This hysteresis property was also shown as the phase  $\delta$  variation of  $\varphi$  oscillation with respect to the field oscillation (Fig. 3a). The micromagnetic simulation result showed almost the same hysteresis behavior (Fig. 3b) with the Duffing oscillator, but it showed fluctuation when the amplitude



and the phase jumped from one stable solution to the other stable line. Note that in Fig. 3 the amplitude is shown with  $\varphi$ . It differs from Fig. 1c, which was plotted with  $I_z (= \sin\theta_0)$ , but the maximum values of  $\varphi_0$  and  $\theta_0$  can be converted through the relation  $N_z \sin^2 \theta_{\max} = N_r \sin^2 \varphi_{\max}$  because the demagnetization energy is alternatively transferred between the  $\hat{z}$  and  $\hat{r}$  directions.

We observed the Duffing-type oscillation and critical field reduction in other radial modes. Figure 4 presents the minimum field for core reversal,  $H_c$ , as a function of frequency  $f$ . To obtain the critical field with fixed frequency, we fixed the external field frequency and varied the amplitude of the field from 0 with a 10 mT/ns rate. Frequency dependent critical field had three local minima and each minimum corresponded to the first, second, and third mode. The obtained  $H_c$  values for modes with fixed frequency were respectively 20 mT for  $n = 1$ , 78 mT for  $n = 2$  mode, and 127 mT for the  $n = 3$  mode. The critical fields were also determined by the sweeping frequency method. For the second mode, the frequency started from 17 GHz with  $-0.2$  GHz/ns sweeping rate; for the third mode, it started from 24 GHz with the same rate. Then, the critical field was 8.5 mT for  $n = 1$ , 37 mT for  $n = 2$ , and 76 mT for  $n = 3$ , which were almost half the values obtained with fixed frequency. The sweeping rate can change the critical field but the variation is small. For example,  $n = 1$  mode,  $H_c = 8.3$  mT with 0.1 GHz/ns rate and 8.6 mT with 0.4 GHz/ns rate. The critical field is obtained with 0.1 mT field interval for  $n = 1$  and 1 mT interval for  $n = 2, 3$ . We confirmed that these reduced critical fields were not achieved through the upward sweeping of the field frequency because of the Duffing-type nonlinear oscillation. In addition, further reduction of the critical field was achieved by using a square wave type external field. For  $n = 1$  mode, we obtained 6.3 mT for the vortex core reversal.

We tested the scalability of the radial mode-induced core reversal. When the radius of the disk was 120 nm, the critical field obtained by the frequency sweeping method was 9.3 mT. The core of a disk with radius 250 nm reverses its polarity with 12 mT external field. Increasing the radius, the critical field also increases. This scalability is an important property for developing data storage devices. Contrary to the radial mode-induced polarity switching, the critical field with the gyration-induced polarity switching exhibits inverse radius dependence<sup>19</sup> as well as the chirality reversal<sup>13</sup>.

Finally, we point out the chaotic behavior and the phase commensurability in the radial mode oscillation for further studies. Petit-

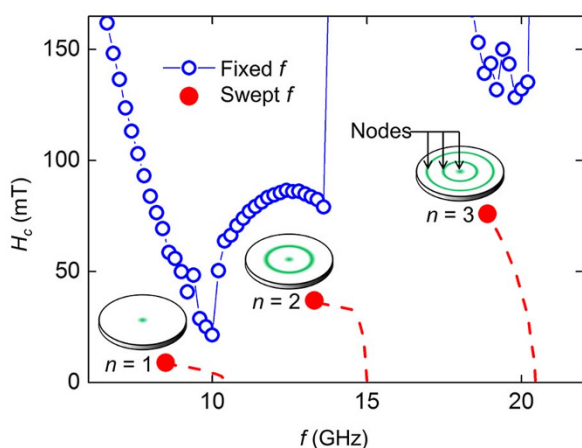


**Figure 4** | Critical fields for the core reversal  $H_c$  with respect to the field frequency  $f$ . The fixed  $f$  results were obtained by amplitude sweeping simulations and the results show three local minima that correspond to each radial mode ( $n = 1, 2, 3$ ); (●) denotes the critical fields determined by the sweeping frequency method; dashed lines represent the maximum amplitude–frequency points in the sweeping method.

Watelot *et al.* observed the chaos and phase-locking phenomenon in the vortex gyration with the core reversal<sup>31</sup>. We observed similar behavior in radial mode oscillation. It is expected that a nonlinear oscillator with a sufficiently large driving force would exhibit chaotic motion. We confirmed this chaotic behavior in the radial mode of the vortex. When the oscillating field strength was smaller than  $H_c$ , a plot of the variable with respect to its time derivative, for example  $\langle \dot{m}_z \rangle$  versus  $\langle m_z \rangle$ , showed a circular trajectory. But when the field was larger than  $H_c$ , this plot becomes complex in the phase space, which manifests its chaotic behavior. Figure 5 shows examples of the chaos in the radial mode. The frequency was fixed at 13.5 GHz. When  $H = 60$  mT  $< H_c$  (Fig. 5a), it showed a closed circular trajectory, but when  $H = 90$  mT  $> H_c$  the trajectory was not closed (Fig. 5b). Further increases in the field resulted in closed trajectories. However, the trajectories were not a simple circle. To close the trajectory, 14 cycles of field oscillation are needed (Fig. 5c) and during these 14 cycles, the core reversed four times. In the case of  $H = 120$  mT, core reversal occurred twice in five field oscillations (Fig. 5d), implying that the core reversal rate was related to the chaotic behavior. Thus, to describe the radial mode of vortex including its chaotic behavior, the core polarity-related term<sup>32</sup> is needed in the motion equation.

In summary, we studied the nonlinear resonance of the radial mode of the vortex and found that the oscillation mode corresponding to the Duffing-type nonlinear oscillator exhibited a hysteresis behavior with respect to the external field frequency. Through the hysteresis effect, we can achieve hidden amplitude that is almost double that obtained with fixed field frequency and this amplitude multiplication effect reduces the critical field below 10 mT. In addition, we pointed out the chaotic behavior of the radial mode for further studies. We think that to complete the study on vortex dynamics, it is timely to start research on the nonlinear behavior in radial modes, as well as in other oscillations of the magnetic vortex.

## Methods

**Micromagnetic simulations.** We performed a micromagnetic simulation using the OOMMF code<sup>26</sup> for numerical calculation of the LLG equation. The simulation structure is a circular disk with a diameter of 160 nm and 7 nm thickness,  $t_{\text{th}}$ , as shown in Fig. 1a. The structure is divided into  $2 \times 2 \times 7$  nm<sup>3</sup> unit cells. Uniform magnetization was assumed along the thickness direction. The material parameters were chosen to resemble a typical permalloy with no crystal anisotropy. The saturation magnetization,  $M_s$ , was  $8.6 \times 10^5$  A/m, the exchange stiffness,  $A$ , was  $1.3 \times$

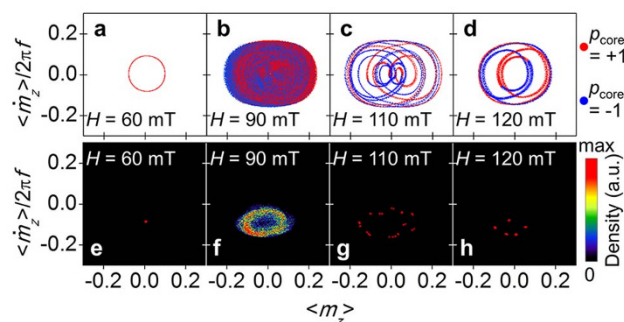


**Figure 5** | Chaotic behaviors of the radial mode oscillation on the phase space. The external field frequency was 13.5 GHz. Phase space plots of  $\langle \dot{m}_z \rangle$  are shown in (a–d). We used different colors, red and blue, to distinguish the core polarization. (e–h), Poincaré sections with zero phase ( $\delta = 0$ ). To obtain a steady state trajectory, simulation data from 10 to 20 ns was plotted, except for (b) and (f). We plotted (b) and (f) with the data from 10 to 500 ns. (a), When the applied field strength is smaller than  $H_c$ , the trajectory resembles a closed circle and the Poincaré section is a single point (e). (b), The trajectory fills some area of the phase space with the increased field. (c), (d), Further increase of the field results in closed trajectories, but they do not show a simple circle. The numbers of points in the Poincaré section represent the number of field cycles needed to close the trajectories.



$10^{-11}$  J/m, and the damping constant  $\alpha$  was 0.01. Then, the magnetization state of the structure had a well-known vortex state composed of a perpendicularly magnetized core at the center of the sample and curling magnetizations around the core. The oscillating external field was applied to the thickness direction, and then the field mainly excited the radial mode that also had axial symmetry.

- Miltat, J. & Thiaville, A. Vortex cores—smaller than small. *Science* **298**, 555 (2002).
- Wachowiak, A. *et al.* Direct observation of internal spin structure of magnetic vortex cores. *Science* **298**, 577 (2002).
- Tchernyshyov, O. & Chern, G.-W. Fractional vortices and composite domain walls in flat nanomagnets. *Phys. Rev. Lett.* **95**, 197204 (2005).
- Choe, S.-B. *et al.* Vortex core-driven magnetization dynamics. *Science* **304**, 420 (2004).
- Im, M.-Y. *et al.* Symmetry breaking in the formation of magnetic vortex states in a permalloy nanodisk. *Nature Comm.* **3**, 983 (2012).
- Van Waeyenberge, B. *et al.* Magnetic vortex core reversal by excitation with short bursts of an alternating field. *Nature* **444**, 461 (2006).
- Vansteenkiste, A. *et al.* X-ray imaging of the dynamic magnetic vortex core deformation. *Nature Phys.* **5**, 332 (2009).
- Pigeau, B. *et al.* A frequency-controlled magnetic vortex memory. *Appl. Phys. Lett.* **96**, 132506 (2010).
- Pigeau, B. *et al.* Optimal control of vortex-core polarity by resonant microwave pulses. *Nature Phys.* **7**, 26 (2011).
- Yu, Y.-S., Jung, H., Lee, K.-S., Fischer, P. & Kim, S.-K. Memory-bit selection and recording by rotating fields in vortex-core cross-point architecture. *Appl. Phys. Lett.* **98**, 052507 (2011).
- Schneider, M., Hoffmann, H. & Zweck, J. Magnetic switching of single vortex permalloy elements. *Appl. Phys. Lett.* **79**, 3113 (2001).
- Tóbiš, J., Cambel, V. & Karapetrov, G. Dynamics of vortex nucleation in nanomagnets with broken symmetry. *Phys. Rev. B* **86**, 134433 (2012).
- Uhlir, V. *et al.* Dynamic switching of the spin circulation in tapered magnetic nanodisks. *Nature Nanotech.* **8**, 341 (2013).
- Okuno, T., Shigeto, K., Ono, T., Mibu, K. & Shinjo, T. MFM study of magnetic vortex cores in circular permalloy dots: behavior in external field. *J. Magn. Magn. Mater.* **240**, 1 (2002).
- Thiaville, A., García, J. M., Dittrich, R., Miltat, J. & Schrefl, T. Micromagnetic study of Bloch-point-mediated vortex core reversal. *Phys. Rev. B* **67**, 094410 (2003).
- Wang, R. & Dong, X. Sub-nanosecond switching of vortex cores using a resonant perpendicular magnetic field. *Appl. Phys. Lett.* **100**, 082402 (2012).
- Yoo, M.-W., Lee, J. & Kim, S.-K. Radial-spin-wave-mode-assisted vortex-core magnetization reversals. *Appl. Phys. Lett.* **100**, 172413 (2012).
- Xiao, Q. F., Rudge, J., Choi, B. C., Hong, Y. K. & Donohoe, G. Dynamics of vortex core switching in ferromagnetic nanodisks. *Appl. Phys. Lett.* **89**, 262507 (2006).
- Lee, K.-S. *et al.* Universal criterion and phase diagram for switching a magnetic vortex core in soft magnetic nanodots. *Phys. Rev. Lett.* **101**, 267206 (2008).
- Hertel, R., Gilga, S., Fähnle, M. & Schneider, C. M. Ultrafast nanomagnetic toggle switching of vortex cores. *Phys. Rev. Lett.* **98**, 117201 (2007).
- Yu, Y.-S. *et al.* Resonant amplification of vortex-core oscillations by coherent magnetic-field pulses. *Sci. Rep.* **3**, 1301 (2013).
- Kravchuk, V. P., Sheka, D. D., Gaididei, Y. & Mertens, F. G. Controlled vortex core switching in a magnetic nanodisk by a rotating field. *J. Appl. Phys.* **102**, 043908 (2007).
- Kammerer, M. *et al.* Magnetic vortex core reversal by excitation of spin waves. *Nature Comm.* **2**, 279 (2011).
- Buess, M. *et al.* Fourier transform imaging of spin vortex eigenmodes. *Phys. Rev. Lett.* **93**, 077207 (2004).
- Guslienko, K. Y., Scholz, W., Chantrell, R. W. & Novosad, V. Vortex-state oscillations in soft magnetic cylindrical dots. *Phys. Rev. B* **71**, 144407 (2005).
- Donahue, M. J. & Porter, D. G. *OOMMF User's Guide, Version 1.2a4*, Interagency Report NISTIR 6376 (National Institute of Standards and Technology, 1999).
- Tretiakov, O. A., Clarke, D., Chern, G.-W., Bazaliy, Y. B. & Tchernyshyov, O. Dynamics of domain walls in magnetic nanostrips. *Phys. Rev. Lett.* **100**, 127204 (2008).
- Nayfeh, A. H. & Mook, D. T. *Nonlinear Oscillations* (Wiley, 1995).
- Aldridge, J. S. & Cleland, A. N. Noise-enabled precision measurements of a Duffing nanomechanical resonator. *Phys. Rev. Lett.* **94**, 156403 (2005).
- Unterreithmeier, Q. P., Faust, T. & Kotthaus, J. P. Nonlinear switching dynamics in a nanomechanical resonator. *Phys. Rev. B* **81**, 241405(R) (2010).
- Petit-Watelot, S. *et al.* Commensurability and chaos in magnetic vortex oscillations. *Nature Phys.* **8**, 682 (2012).
- Pylypovskii, O. V., Sheka, D. D., Kravchuk, V. P., Mertens, F. G. & Gaididei, Y. Regular and chaotic vortex core reversal by a resonant perpendicular magnetic field. *Phys. Rev. B* **88**, 014432 (2013).

## Acknowledgments

This research was supported by the International Research and Development Program of the National Research Foundation of Korea (NRF) funded by the Ministry of Science, ICT and Future Planning of Korea (grant number: 2012-00156, FY 2012).

## Author contributions

C.H. and K.-W.M. designed the project and C.H. coordinated the project. K.-W.M. carried out the micromagnetic simulations and analyzed the data. K.-W.M., C.H. and Z.Q.Q. wrote the manuscript with the help of B.-S.C. and W.K. All the authors discussed the data and commented on the manuscript.

## Additional information

**Competing financial interests:** The authors declare no competing financial interests.

**How to cite this article:** Moon, K.-W., Chun, B.S., Kim, W., Qiu, Z.Q. & Hwang, C. Duffing oscillation-induced reversal of magnetic vortex core by a resonant perpendicular magnetic field. *Sci. Rep.* **4**, 6170; DOI:10.1038/srep06170 (2014).



This work is licensed under a Creative Commons Attribution-NonCommercial-NoDerivs 4.0 International License. The images or other third party material in this article are included in the article's Creative Commons license, unless indicated otherwise in the credit line; if the material is not included under the Creative Commons license, users will need to obtain permission from the license holder in order to reproduce the material. To view a copy of this license, visit <http://creativecommons.org/licenses/by-nc-nd/4.0/>